ANALYTICAL CALCULATION OF SKIN AND PROXIMITY EFFECTS IN THE PRIMARY WINDING OF A PULSE TRANSFORMER

Belkacem Bouaoune[1,2], Yves Mulet Marquis[2], Yves Bernard[1]

[1]Laboratoire de Génie Electrique de Paris LGEP-SUPELEC,
11 rue Joliot-Curie, 91192 Gif-sur-Yvette CEDEX, France
[2]LACMÉ S.A.S.,
Route du Lude – Les Pelouses 72200 La Flèche, France

bouaoune@lgep.supelec.fr (Belkacem Bouaoune)

Abstract

This article deals with the analytical modelling of skin and proximity effects present in windings of the electric machines. The selected application is the primary winding of a pulse transformer. An example of a real pulse transformer is studied. The analytical expression giving the space-time distribution of the flux density, in the case of an idealized winding layer of semi-infinite plane geometry, has been established first. The current density calculation based on the established formula giving the flux density makes it possible to estimate the primary winding DC resistance, and then the Joule losses in the transformer primary winding. The losses found in the primary winding of the studied transformer using the established formula are quite higher than what they would be if the current was distributed uniformly in the conductors. In fact, the effective resistance of the transformer primary winding calculated using our model is about 40% higher than the calculated continuous resistance. This result has also been verified indirectly experimentally. The analytical model is validated thereafter by a discrete modelling methodology which consists in an electrical equivalent circuit [1]. The results given by the analytical modelling are perfectly identical to those of the discrete modelling presented in [1] for the same example studied.

Keywords: Pulse transformer, Skin and proximity effects, Transformer Joule losses

Presenting Author's biography

Yves Mulet Marquis was born in France in 1946. After more than 20 years of experience in the fields of power electronics and low power electric motor drives, he joined LACME SAS as chief engineer in 1993. Then he works on the various design aspects of electric fence energizers and lead acid battery chargers. He also becomes an active member of electrical safety standardization committees at the UTE, CENELEC and IEC level. Mr. Mulet Marquis holds several French and international patents on low power electric motor drives, fence energizers and battery chargers.

1   Introduction

In [1], the authors showed that an equivalent circuit model can be used in order to estimate the skin and proximity effects in the primary winding of a pulse transformer. Their model allows obtaining a first estimation of the AC resistance when the layer is excited by a rapidly changing current. Moreover, the model can take into account any temporal form of excitation. However, the integration of such a method in the algorithms calculating the losses in the transformer windings will remain, in our opinion, a tedious work because it would imply the combination of a software interface of electric circuits calculation and a programming environment.

In another paper [2], the same authors developed an analytical model which accounts for the phenomenon of the magnetic field penetration in the core laminations of magnetic circuits. In fact, they established an analytical expression giving the space-time distribution of the magnetic flux density within a lamination excited on both sides of its surfaces by an unspecified temporal form signal. However, the mathematical formalism such developed in [2] for the phenomenon of the magnetic field penetration is unfortunately not adapted for the problem studied in this paper. In fact, the boundary conditions are different when dealing with an idealized magnetic lamination where the magnetic field on the two sides of its surfaces is the same one (Fig. 1), or in the case of an idealized layer of winding where the magnetic field on the two sides of each winding layer is different (Fig. 2).
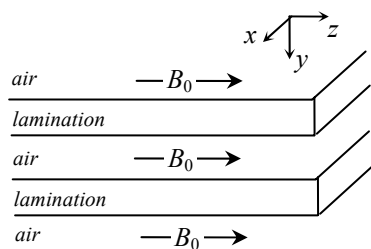

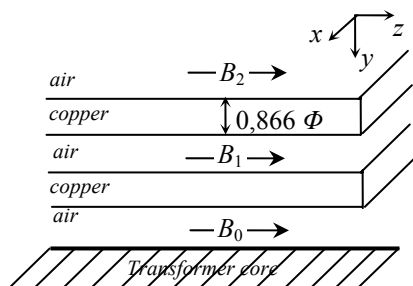Fig. 1: Idealized geometry of a lamination

Fig. 2: Idealized plane primary winding

In order to be able to exploit the methodology developed in [2] and thus to establish an analytical expression calculating the skin and proximity effects

in the transformer winding, we must find a mathematical analogy between the problem of the skin and proximity effects in the transformer winding and that of the magnetic field penetration in the core laminations. This is related, in fact, to the boundary conditions on the external surfaces of each layer. The magnitude of the excitation must be indeed of the same value on both sides of the equivalent conducting ribbon.

Let's consider the case of the semi-infinite plane geometry defined by Harrison in [3]. The made assumptions are as follow: The flux density has only one component which is directed along z-axis, the current density has only one component directed along x-axis, the values of the current and flux densities depend only on the depth y in the conductor and on the time t. One assimilate the conductors of a layer to a semi-infinite ribbon thickness $2a$ similar to that defined by Dowell [4]. One side of the conducting ribbon is positioned at $y = a$, and the other side at $y = -a$ (Fig. 3).

Firstly, we will determine the response of the conducting ribbon subjected on both sides of its surfaces to two constant induction levels having different magnitudes. Further, we will use the methodology developed in [2] to determine the response of this conducting ribbon when the two excitations are of an unspecified temporal form. Thus, knowing the analytical expression giving the space-time distribution of the flux density inside the ribbon, the skin and proximity effects can be evaluated by calculating the current densities in all points inside the ribbon and at all times.

2   Response to constant induction levels having different magnitudes

At the beginning, one applies an induction level of amplitude B_+ on the face $y = a$ of the conducting ribbon and an induction level of amplitude B_- on the face $y = -a$ (Fig. 3).
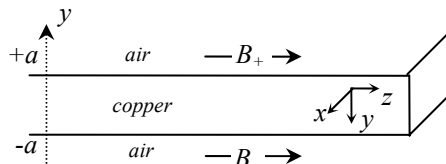

Fig. 3: Boundary conditions B_+ and B_-

Mathematically speaking, the application of these two induction levels can also be interpreted as the sum of an even excitation and an odd excitation. The even excitation is the application of two induction levels having the same magnitude. This is given by (1).

$$B_p = \frac{B_+ + B_-}{2} \qquad (1)$$

The odd excitation is the application of two induction levels having an opposite magnitude. This is given by (2).

$$B_i = \frac{B_+ - B_-}{2} \qquad (2)$$

According to the superposition principle, the total response of the conducting ribbon will be the sum of the responses of the even and the odd excitations.

The partial derivative Maxwell's equations, which obey the flux and the current densities are given by (3) and (4) within the framework of the assumptions made for the selected geometry.

$$\frac{\partial^2 B_z(y,t)}{\partial y^2} = \sigma\mu \frac{\partial B_z(y,t)}{\partial t} \qquad (3)$$

$$\frac{\partial J_x(y,t)}{\partial y} = \sigma \frac{\partial B_z(y,t)}{\partial t} \qquad (4)$$

2.1 Response to the even excitation

The excitation being independent of time, after extinction of the transient state the flux density distribution $B_{zp}(y)$ in the conducting ribbon must also be independent of time. One obtains (5) by taking into account the Maxwell's equations and the boundary conditions at $y = a$ and $y = -a$.

$$B_{zp}(y) = B_p \, \xi(t) \qquad (5)$$

Where $\xi(t)$ is the unit level.

It is shown in [3] that the general solutions depending on time of the equations (3) and (4) are of the following form:

$$B_{zp}(y,t) = B_a \sum_k \left\{ \left(A\cos(ky) + B\sin(ky) \right) \right.$$
$$\left. \exp\!\left(\frac{-k^2 t}{\sigma\mu} \right) \right\} \quad (6)$$

The complete solution giving the response to the even excitation is the sum of the solution independent of time and the general solutions dependent on time (7).

$$B_{zp}(y,t) = B_a \sum_k \left\{ \xi(t) + \left(A\cos(ky) \right. \right.$$
$$\left. \left. + B\sin(ky) \right)\exp\!\left(\frac{-k^2 t}{\sigma\mu} \right) \right\} \quad (7)$$

At the initial moment, the flux density is not established immediately inside the conducting ribbon. $B_{zp}(y,0)$ will be thus null whatever the depth in the

conducting ribbon except at its boundaries where the flux density is equal to B_p.

In order to satisfy these boundary conditions at the initial time, the flux density $B_{zp}(y,0)$ is approached by the opposite of a periodic function $f(y)$ of which the period is $4a$ (Fig. 4). This function will thus be worth 1 between $y = -a$ and $y = a$, except at the ends of the interval to preserve the value of the excitation B_p.

$$f(y) = \sum_{n=1}^{\infty} -a_{2n} \cos\!\left(\frac{\pi a_{1n}}{2a} y \right) \qquad (8)$$

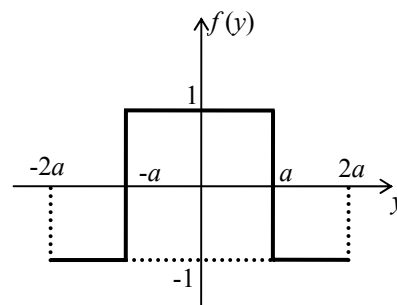Où : $a_{1n} = (2n-1)$ et $a_{2n} = (-1)^n \, 4/\pi a_{1n}$

Fig. 4: Function defining the boundary conditions at the initial time relating to the even excitation

These boundary conditions make it possible to fix at the same occasion the coefficients *A*, *B* and *k* of (7). One thus obtains the analytical solution giving the response to the even excitation (9).

$$B_{zp}(y,t) = B_p \left\{ \xi(t) + \sum_{n=1}^{\infty} f_{np}(t)\, g_{np}(y) \right\} \qquad (9)$$

Where: $\tau_m = \sigma\mu \left(\frac{2a}{\pi} \right)^2$, $f_{np}(t) = a_{2n} \exp\!\left(-\frac{a_{1n}^2 t}{\tau_m} \right)$

and $g_{np}(y) = \cos\!\left(\frac{\pi a_{1n}}{2a} y \right)$

2.2 Response to the odd excitation

The excitation being independent of time, after extinction of the transient state the flux density distribution $B_{zi}(y)$ in the conducting ribbon must also be independent of time. One obtains (10) by taking into account the Maxwell's equations and the boundary conditions at $y = a$ and $y = -a$.

$$B_{zp}(y) = B_i \, \xi(t) \left(\frac{y}{a} \right) \qquad (10)$$

The complete solution giving the response to the odd excitation is the sum of the solution independent of time and the general solutions dependent on time (11).

$$B_{zp}(y,t) = B_a \sum_j \left\{ \xi(t)\left(\frac{y}{a}\right) + (C\cos(jy) + D\sin(jy))\exp\left(\frac{-J^2 t}{\sigma\mu}\right) \right\} \quad (11)$$

In the same way, as for the even excitation at the initial moment, the flux density is not established immediately inside the conducting ribbon. $B_{zi}(y,0)$ will be thus null whatever the depth in the conducting ribbon except at its boundaries where the flux density is equal to B_i.

In order to satisfy also these boundary conditions at the initial time, the flux density $B_{zi}(y,0)$ is approached by the opposite of a periodic function $l(y)$ (Fig. 5). This function is linear between $y = -a$ and $y = a$, and worth respectively at these points -1 and 1. That makes it possible to preserve at the ends of the interval the values of the odd excitation B_i.

$$l(y) = \sum_{n=1}^{\infty} \frac{-2(-1)^n}{n\pi} \sin\left(\frac{n\pi}{a}y\right) \quad (12)$$
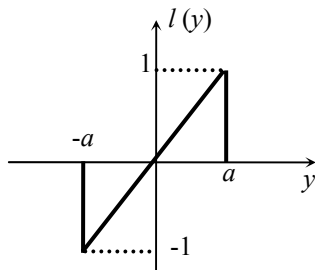
Fig. 5: Function defining the boundary conditions at the initial time relating to the odd excitation

In the same way, these boundary conditions make it possible to fix at the same occasion the coefficients *C*, *D* and *j* of (11). One thus obtains the analytical solution giving the response to the odd excitation (13).

$$B_{zi}(y,t) = B_i \left\{ \xi(t)\left(\frac{y}{a}\right) + f_{ni}(t) g_{ni}(y) \right\} \quad (13)$$

Where: $f_{ni}(t) = (-1)^n \frac{2}{n\pi} \exp\left(-\frac{4n^2 t}{\tau_m}\right)$

and $g_{ni}(y) = \sin\left(\frac{n\pi}{a}y\right)$

2.3 Total response

The total response of the conducting ribbon thickness $2a$ to the constant induction levels of unequal magnitudes, applied on both sides of its two external surfaces, will be thus under the terms of the superposition principle equal to the sum of the responses to the even and the odd excitations (14).

$$B_z(y,t) = B_{zp}(y,t) + B_{zi}(y,t) \quad (14)$$

That gives by the substitution of (9) and (13) in (12) the total response (15).

$$B_z(y,t) = B_p \left\{ \xi(t) + \sum_{n=1}^{\infty} f_{np}(t) g_{np}(y) \right\} + B_i \left\{ \xi(t)\left(\frac{y}{a}\right) + \sum_{n=1}^{\infty} f_{ni}(t) g_{ni}(y) \right\} \quad (15)$$

2.4 Numerical example

To validate the analytical expressions giving the space-time distribution of the flux density inside the conducting ribbon, we will treat as example the case of a ribbon excited by two constant induction levels $B_+ = 2\,\text{T}$ and $B_- = 0\,\text{T}$. That gives according to (1) and (2): $B_p = B_i = 1\,\text{T}$.

We will apply these excitation conditions to the first layer of the pulse transformer primary winding treated in [1]. This winding is equivalent to a conducting ribbon thickness $2a = 0{,}886$ mm having an equivalent conductivity $\sigma_2 = 47{,}37\,10^6$ S [4]. The permeability of the conducting ribbon is $\mu = \mu_0 = 4\pi\,10^{-7}$.

The results of the analytical model are compared with those of the discrete model developed in [1]. The assumptions made for the development of the discrete model are identically the same one as those done for the analytical model. The diagram of the discrete simulation is given by (Fig. 6).
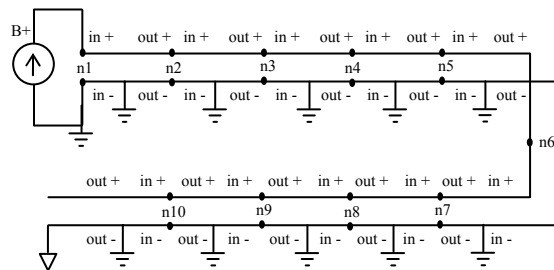
Fig. 6: Diagram simulating the internal layer of the transformer primary winding

Each symbol of (Fig. 6) is constituted of a cell <in+ out+, in- out-> contains 10 multiple cells, and each multiple cell contains 10 basic cells. The basic

cells are defined by an RL circuit such shown by (Fig. 7). The conductance G is the inverse of a resistance R. Knowing that a basic cell represents a hundredth thickness of the equivalent conducting ribbon, and that the equivalent thickness of the ribbon is equal to $0,886\ \Phi$ [4] (where Φ is the conductor diameter), the element dy will thus be worth $0,886\ \Phi/100$. According to [1] the inductance L and the conductance G of (Fig. 7) worth respectively σ_2 and μ_0.
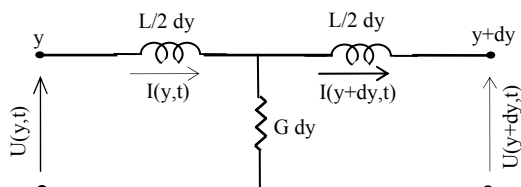

Fig. 7: Basic cell

The current sources representing by identification the flux densities at the lower and higher boundaries of the ribbon are respectively B_+ and B_- (Fig. 3). The source B_- is represented by an open circuit, because the current is null (Fig. 6).

Figure 8 shows the flux densities in the conducting ribbon for some different duration of the applied induction levels. The full curves result from the analytical modelling where the expression of $B_z(y,t)$ given by (15) was evaluated with $n = 100$ terms. The points result from the discrete modelling.
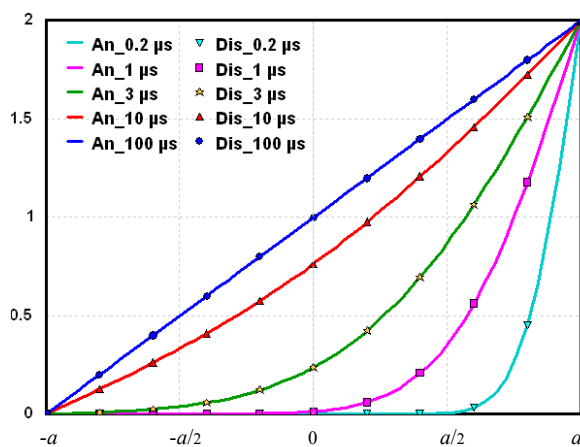
Fig. 8: Induction penetration according to the depth in the conducting ribbon thickness $2a$, Tesla

The agreement between the two models is excellent (Fig. 8). In fact, the points and the curves are perfectly superimposed. That validates our analytical approach in the case of an excitation by dissymmetric induction levels.

3 Response to excitations of unspecified temporal forms

The Maxwell's equations are linear. The superposition principle can thus be applied. Thus, the response of a conducting ribbon subjected to a sum of excitations will be the sum of the responses to each excitation taken individually. By using this principle and the results of the preceding section, we will show, as in [2] by two different methods of calculation, how to lead to the analytical formulation of the flux density in a conducting ribbon subjected on both sides of its surfaces to a magnetic excitation of unspecified temporal form.

3.1 Summation of rectangular pulses

A rectangular pulse of magnitude B_a and width Δt is equivalent to a constant level of magnitude B_a applied at t_0 followed by a constant level of magnitude $-B_a$ applied at $t_0 + \Delta t$ (Fig. 9).
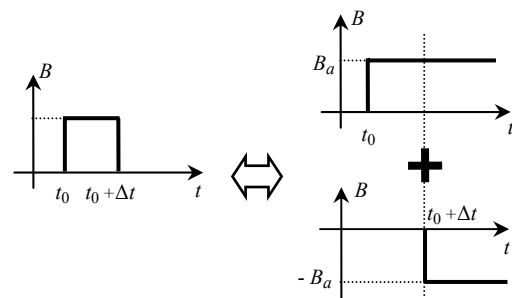

Fig. 9: Decomposition of a rectangular pulse in constant levels

Knowing the response of the ribbon subjected on both sides of its surfaces to the even constant level B_p given by (9), the response which one will obtain in the case of a rectangular pulse of magnitude B_p will thus be given by (16).

$$B_{zp}(y,t) = B_p \left\{ \xi(t-t_0) + \xi(t-(t_0+\Delta t)) \right.$$
$$\left. + \sum_{n=1}^{\infty} \left[f_{np}(t-t_0) - f_{np}(t-(t_0+\Delta t)) \right] g_{np}(y) \right\} \quad (16)$$

In the same way, starting from (13) the response to the rectangular odd excitation of magnitude B_i will be given by (17).

$$B_{zi}(y,t) = B_i \left\{ \left[\xi(t-t_0) + \xi(t-(t_0+\Delta t)) \right] \left(\frac{y}{a} \right) \right.$$
$$\left. + \sum_{n=1}^{\infty} \left[f_{ni}(t-t_0) - f_{ni}(t-(t_0+\Delta t)) \right] g_{ni}(y) \right\} \quad (17)$$

A signal of unspecified temporal form can be divided up into rectangular pulses of different magnitudes and equal widths (Fig. 10).
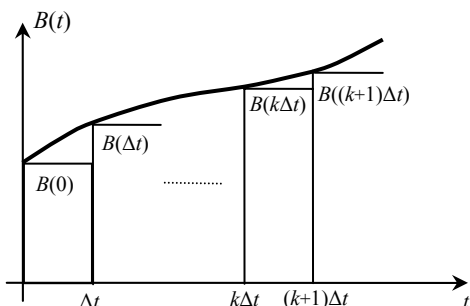

Fig. 10: Division of an unspecified temporal form signal in rectangular pulses

Knowing the responses of the ribbon subjected on both sides of its surfaces to the even and the odd rectangular pulses given respectively by (16) and (17), the responses which one obtains in the case of a sum of rectangular pulses forming the even and the odd excitations of unspecified temporal form will be given respectively by (18) and (19).

$$B_{zp}(y,t) = \sum_{k=1}^{\infty} \left\{ B_p(u)\Delta t \left[\delta(t-u) \right. \right. $$
$$\left. \left. + \sum_{n=1}^{\infty} f_{np}'(t-u)g_{np}(y) \right] \right\} \quad (18)$$

$$B_{zi}(y,t) = \sum_{k=1}^{\infty} \left\{ B_i(u)\Delta t \left[\delta\left(t-u\frac{y}{a}\right) \right. \right. $$
$$\left. \left. + \sum_{n=1}^{\infty} f_{ni}'(t-u)g_{ni}(y) \right] \right\} \quad (19)$$

Where : $u = k\,\Delta t$

$\delta(t-u) = \xi'(t-u)$: Dirac pulse

$\xi'(t-u)$, $f_{np}'(t-u)$ and $f_{ni}'(t-u)$ are respectively the limited developments to the first order of $\xi(t-u)$, $f_{np}(t-u)$ and of $f_{ni}(t-u)$.

Making tend Δt towards zero by the passage to the limit, the sums on k in the expressions (18) and (19) become integrals. And then, by adding the two resulting expressions, one obtains according to (14) the exact analytical expression of the flux density in the conducting ribbon subjected on both sides of its surfaces to two dissymmetrical excitations of unspecified temporal forms (20).

$$B_z(y,t) = \int_0^{\infty} \left\{ B_p(u) \left[\delta(t-u) + \sum_{n=1}^{\infty} f_{np}'(t-u)g_{np}(y) \right] \right. $$
$$\left. + B_i(u) \left[\delta\left(t-u\left(\frac{y}{a}\right)\right) + \sum_{n=1}^{\infty} f_{ni}'(t-u)g_{ni}(y) \right] \right\} du \quad (20)$$

3.2 Summation of constant levels

A signal of unspecified temporal form can also be approached by a sum of constant levels with different magnitudes shifted regularly in time (Fig.11).
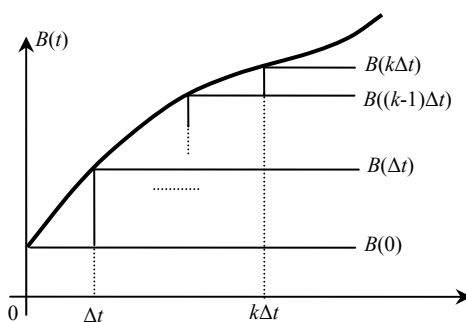

Fig. 11: Division of an unspecified temporal form signal in constant levels signals

One can there too apply the superposition principle to find the exact analytical expression of the flux density in the conducting ribbon subjected to the even and the odd excitations. In fact, we can add all the constant levels resulting from the division of the two basic signals by using the expression (15). And after, by making tend towards zero by the passage to the limit, the sums on k in the resulting expressions become integrals, and thus give the exact analytical expression of the flux density in the conducting ribbon subjected on both sides of its surfaces to two dissymmetrical excitations of unspecified temporal forms (21).

$$B_z(y,t) = B_p(0)\left[\xi(t) + \sum_{n=1}^{\infty} f_{np}(t)\,g_{np}(y) \right] $$
$$+ \int_0^{\infty} B_p'(u)\left[\xi(t-u) + \sum_{n=1}^{\infty} f_{np}(t-u)\,g_{np}(y) \right] du $$
$$+ \int_0^{\infty} B_i'(u)\left[\xi(t-u)\left(\frac{y}{a}\right) + \sum_{n=1}^{\infty} f_{ni}(t-u)\,g_{ni}(y) \right] du $$
$$+ B_i(0)\left[\xi(t)\left(\frac{y}{a}\right) + \sum_{n=1}^{\infty} f_{ni}(t)\,g_{ni}(y) \right] \quad (21)$$

$B_p'(u)$ and $B_i'(u)$ are respectively the limited developments to the first order of $B_p(u)$ and of $B_i(u)$.

If the even and the odd excitations have a null initial value, the preceding expression (21) will be reduced to (22).

$$B_z(y,t) = \int_0^\infty \left\{ B_p'(u) \left[\xi(t-u) + \sum_{n=1}^\infty f_{np}(t-u)\, g_{np}(y) \right] \right.$$

$$\left. + B_i'(u) \left[\xi(t-u)\left(\frac{y}{a}\right) + \sum_{n=1}^\infty f_{ni}(t-u)\, g_{ni}(y) \right] \right\} du \quad (22)$$

4 Concrete example – Pulse Transformer

4.1 Flux and current densities calculation in the equivalent conducting ribbon

Using the second method (summation of constant levels), we will treat the case of the first layer of the pulse transformer primary winding studied in [1]. This transformer comprises $n_1 = 1000$ turns at the secondary and $n_2 = 40$ turns at the primary. The diameter of the primary winding wire is $\Phi_1 = 1,12$ mm and the distance between the centres of two adjoining wires is $d_1 = 1,217$ mm . The number of turns per meter at the primary winding is $n = 1/d_1$.

Using the transformation defined by Dowell [4], the ribbon thickness equivalent to the first layer of the primary winding will be equal to $0,886\,\Phi_1$ and the equivalent conductivity of the ribbon which will make it possible to keep the same value of the resistance will be $\sigma_2 = 0,886\,\Phi_1 \sigma_1/d_1$. The conductivity σ_1 of the cylindrical conductors is that of copper ($58,1\ 10^6$ S) and their magnetic permeability is $\mu = \mu_0$.

In the case of our transformer, the output voltage pulse is known and assimilated to an exponential pulse (23). The parameters U_{20}, τ_1 and τ_2 are adjusted to approach as closer as possible the real forms of output voltage pulses that are measured. So be it $U_{20} = 25$ kV , $\tau_1 = 20\,\mu s$ and $\tau_2 = 35\,\mu s$ on a purely resistive load at the secondary side $R_2 = 1\,k\Omega$.

$$U_2(t) = U_{20} \exp\left(-\frac{t}{\tau_2}\right)\left(1 - \exp\left(-\frac{t}{\tau_1}\right)\right) \quad (23)$$

By supposing an infinite permeability of the transformer core, the source of induction representing the lower boundary condition of the primary winding internal layer (Fig. 3) will be given by (24).

$$B_-(t) = 0 \quad (24)$$

By applying the Ampere theorem one obtains (25).

$$B_+(t) = \mu_0\, n\, i_1(t) \quad (25)$$

Where $i_1(t)$ is the current traversing the conducting ribbon.

The infinite permeability of the core being supposed, the Ampere-turns of the primary and the secondary windings are then equal. Thus, for a purely resistive load at the secondary side, the primary current has the form of the output voltage. The induction $B_+(t)$ representing the higher boundary condition of the primary winding first layer will be then given by (26).

$$B_+(t) = \frac{\mu_0\, n_2\, U_{20}}{d_1\, n_1\, R_2} \exp\left(-\frac{-t}{\tau_2}\right)\left(1 - \exp\left(-\frac{-t}{\tau_1}\right)\right) \quad (26)$$

From (1) and (2), and knowing (24) and (26), the even and the odd excitations will thus be given by (27).

$$B_p(t) = B_i(t) = B_m \exp(-\lambda_1 t)\left(1 - \exp\left(-\frac{t}{\tau_1}\right)\right) \quad (27)$$

Where: $B_m = \dfrac{\mu_0\, n_2\, U_{20}}{2 d_1\, n_1\, R_2}$ et $\lambda_1 = \dfrac{1}{\tau_2}$

The derivative calculation of $B_p(t)$ and $B_i(t)$ from (27) gives (28).

$$B_p'(t) = B_i'(t) = B_m \left(\lambda_1 \exp\left(-\lambda_1 t\right) - \lambda_2 \exp\left(-\lambda_2 t\right) \right) \quad (28)$$

Where: $\lambda_2 = \dfrac{\tau_1 + \tau_2}{\tau_1 \tau_2}$

By making a change of variable $t-u = v$ and by noticing that the functions $f_{np}(v)$ and $f_{ni}(v)$ are null for v inferior to zero, and then by substituting (28) in (22) we obtain (29).

$$B_z(y,t) = \int_0^t \left\{ B_m \left[\lambda_1 \exp\left(-\lambda_1(t-v)\right) - \lambda_2 \exp\left(-\lambda_2(t-v)\right) \right] \right.$$

$$\left. \left[\frac{y+a}{a} + \sum_{n=1}^\infty \left(f_{np}(v)\, g_{np}(y) + f_{ni}(v)\, g_{ni}(y) \right) \right] \right\} dv \quad (29)$$

After the calculation of the integral appearing in (29) we end to (30).

Where: $a_{3n} = \dfrac{1}{\left(1 - a_{1n}^2\right)}$

and $a_{4n} = \dfrac{1}{\left(1 - 4n^2\right)}$

$$B_z(y,t)=\left(\frac{B_m(y+a)}{a}\right)(\exp(-\lambda_1 t)+\exp(-\lambda_2 t))+B_m\sum_{n=1}^{\infty}$$

$$\left\{a_{2n}\,g_{np}(y)\left[\lambda_2\tau_m a_{3n}\left(\exp\left(\frac{-a_{1n}^2 t}{\tau_m}\right)-\exp(-\lambda_2 t)\right)\right.\right.$$

$$\left.-\lambda_1\tau_m a_{3n}\exp\left(\frac{-a_{1n}^2 t}{\tau_m}\right)-\exp(-\lambda_1 t)\right]$$

$$+\frac{2(-1)^n}{n\pi}g_{ni}(y)\left[\lambda_2\tau_m a_{4n}\left(\exp\left(\frac{-4n^2 t}{\tau_m}\right)-\exp(-\lambda_2 t)\right)\right.$$

$$\left.\left.-\lambda_1\tau_m a_{4n}\exp\left(\frac{-4n^2 t}{\tau_m}\right)-\exp(-\lambda_1 t)\right]\right\}\quad(30)$$

The space-time distribution of the current density is obtained simply by application of the equation (4). Then, taking into account (30), the current density in the conducting ribbon will be given by (31) in the case of the studied example.

$$J_x(y,t)=\left(\frac{B_m}{\mu a}\right)\left\{(\exp(-\lambda_1 t)+\exp(-\lambda_2 t))+2\sum_{n=1}^{\infty}(-1)^n\right.$$

$$\left\{\cos\left(\frac{n\pi}{a}y\right)\left[\lambda_2\tau_m a_{4n}\left(\exp\left(\frac{-4n^2 t}{\tau_m}\right)-\exp(-\lambda_2 t)\right)\right.\right.$$

$$\left.-\lambda_1\tau_m a_{4n}\exp\left(\frac{-4n^2 t}{\tau_m}\right)-\exp(-\lambda_1 t)\right]$$

$$-\sin\left(\frac{a_{1n}\pi}{2a}y\right)\left[\lambda_2\tau_m a_{3n}\left(\exp\left(\frac{-a_{1n}^2 t}{\tau_m}\right)-\exp(-\lambda_2 t)\right)\right.$$

$$\left.\left.\left.-\lambda_1\tau_m a_{3n}\exp\left(\frac{-a_{1n}^2 t}{\tau_m}\right)-\exp(-\lambda_1 t)\right]\right\}\right\}\quad(31)$$

The figure 12 shows the current densities in the conducting ribbon according to the pulse duration for the following depths: $y = -a$, $y = 0$, $y = a/3$, $y = a/4$ and $y = a$. The full curves result from the analytical modelling where the expression of $J_x(y,t)$ given by (31) was evaluated with $n = 100$ terms. The points result from the discrete modelling where the source B1 of (Fig. 6) is that given by (26).

One can see on (Fig. 2), as in the preceding example, that the agreement between the two models (analytical and discrete) is perfect. That validates definitively our analytical approach in the case of excitations of unspecified temporal forms.
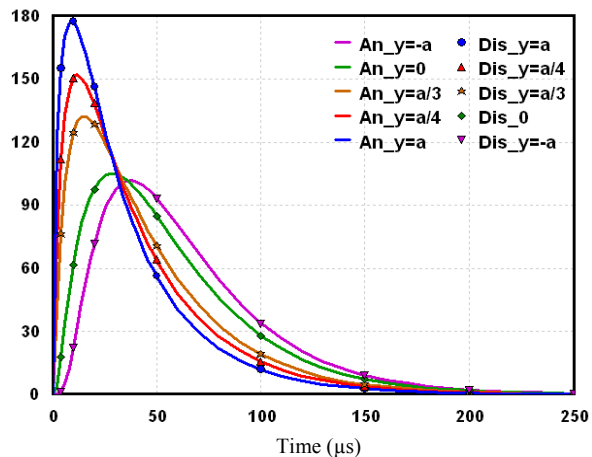

Fig. 12: Current density (A/mm²) for different depths in the conductor thickness 2a

4.2 The Joule losses

The current in a layer thickness dy and width ℓ (Fig. 13) is equal to the flux of the current density through the surface $\ell\,dy$ (32).
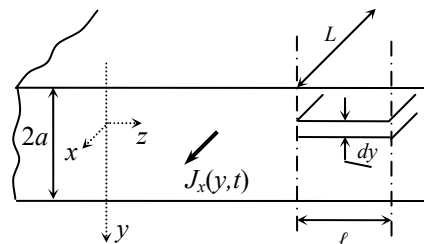
$$dI_1 = J_x(y,t)\ell\,dy\quad(32)$$

Fig. 13: Conducting layer thickness dy

The resistance dR_1 of the layer thickness dy, width ℓ, length L and conductivity σ_2 is given by (33).

$$dR_1 = \frac{1}{\sigma_2}\frac{L}{\ell\,dy}\quad(33)$$

The energy lost by Joule effect during a time dt in the layer thickness dy, width ℓ, length L and conductivity σ_2 is given by (34).

$$d^2E = dR_1(dI_1)^2\,dt\quad(34)$$

By substituting (32) and (33) in (34), the energy lost throughout the pulse of period t_{pulse} on all the thickness of the conducting ribbon will be given by (35).

$$E = \int_0^{t_{pulse}}\frac{2aL\ell}{\sigma_2}\left(\frac{1}{2a}\int_{-a}^{a}J_x^2(y,t)dy\right)\quad(35)$$

The evaluation of (35) in the case of an elementary rectangular conductor of width ℓ equal to the distance between centres of two adjoining turns, gives the energy lost per unit of length in the case of the primary winding internal layer of the studied pulse

transformer: $E = 0{,}02$ J/m. The expression of $J_x(y,t)$ given by (31), in (35) is evaluated with $n = 100$ terms.

If the current had been distributed uniformly in the layer, the losses by Joule effect would have been given by (36).

$$E' = \frac{L}{0{,}886\,\sigma_2\,\ell\,\Phi_1} \int_0^{t_{pulse}} \left\{ \left(\frac{n_2 U_{20}}{n_1 R_2}\right)^2 \exp\left(\frac{-2t}{\tau_2}\right) \right. $$
$$\left. \left(1 - 2\exp\left(\frac{-t}{\tau_1}\right) + \exp\left(\frac{-2t}{\tau_1}\right)\right) \right\} dt \quad (36)$$

The evaluation of (36) in the case of an elementary rectangular conductor of width ℓ equal to the distance between centres of two adjoining turns, gives the energy lost per unit of length in primary winding internal layer of the studied pulse transformer: $E' = 0{,}014$ J/m.

The real losses in the primary winding internal layer of the studied pulse transformer are quite higher than what they would be if the current were distributed uniformly in the conductors and that the proximity effects were neglected. Indeed, the effective resistance of the internal layer is 1,42 times higher than the calculated continuous resistance. In other words, the resistance is increased by 42%.

5   Conclusions

The results of the analytical formulation are identical to those of the discrete model. Actually, these results are hardly surprising since the two models are based on the same assumptions. The comparison allows nevertheless to validate our approach of modelling, and also allows to consolidate the results obtained in [1], in particular concerning the skin and proximity effects absolutely to take into account when designing devices as the one studied in this paper.

The major advantage of this analytical model compared to the discrete model, is the possibility of its insertion rather easily in the algorithms calculating the losses in the windings of transformers.

The use of an idealized geometry far from the concrete reality of the winding undoubtedly limits the method, but the old analytical models use practically the same assumptions. On the other hand, our modelling accepts sources of unspecified temporal forms including pulses. It makes also much more intuitive the reasons of the unequal distribution of the current in the conductors. It is a major advantage compared to the preceding analytical methods which generally suppose sinusoidal periodic signals. They become very heavy for simply periodic signals since it is necessary to divide up the original signal in Fourier series and to study individually the case of each harmonic. They do not give a response for no periodic signals like pulses.

6   References

[1] B. Bouaoune, Y. Mulet Marquis and Y. Bernard. Equivalent diagramm estimation of skin and proximity effects in the primary winding of a pulse transformer. *Paper submitted to ISEF'2007, http://www.isef2007-prague.cz* (Paper accepted for presentation, Prague, September 12 – 15, 07).

[2] B. Bouaoune, Y. Mulet Marquis and Y. Bernard. Analytical solution of the magnetic field diffusion equation in a Lamination temporally excited. *Paper submitted to SMM18 (Soft Magnetic Materials Conference), http:// www.cardiff.ac.uk* (Paper accepted for presentation, Cardiff, September 2 – 5, 2007).

[3] C.B. Harisson. An Analysis of pulse transformers. *Thesis University of Waikato New Zealand, 1998.*

[4] B. Carsten. Calculating skin and proximity effect conductor losses in switch mode magnetics. *Seminar 3 PCIM 94, 1994.*

7   Biographies

Belkacem Bouaoune was born in lowland of Kabylie, Algeria, on Mai 23, 1976. He is working currently as research engineer for LACME SAS, and he pursuing the Ph.D. degree at the Université de Paris XI in the Laboratoire de Génie Electrique de Paris. His interests include modelling, optimization and design of electromagnetic devices.

Yves Bernard was born in Paris in France, on January 8, 1974. He graduated from the University of Paris-Sud Orsay with a diploma in energy transformation. He became a doctor in September 2000 with a thesis about the magnetic hysteresis modelling in finite element modelling method. He is professor assistant at the University of Paris-Sud Orsay since September 2001. His research activity deals with the modelling and conception of electromagnetic devices.